JOURNAL OF Materials CHEMISTRY

Synthesis and electrical properties of the $Pr_{0.5+x+y}Li_{0.5-3x}Ti_{1-3y}Cr_{3y}O_3$ system

M. Morales and M. L. Martínez Sarrión*†

Dept. Inorganic Chemistry, Universitat de Barcelona, Diagonal 647, 08028, Spain

The stoichiometry, polymorphism and electrical behaviour of solid solutions $Pr_{0.5+y+x}Li_{0.5-3x}Ti_{1-3y}Cr_{3y}O_3$ with perovskite-type structure have been studied. Data are given in the form of a solid solution triangle, phase diagrams, XRD patterns for the three polymorphs, A, β, and C, composition dependence of their lattice parameters and ionic and electronic conductivity plots. Microstructure and composition were studied by SEM/EDS and electron probe microanalysis. These compounds are mixed conductors. Ionic conductivity decreased when the amount of lithium diminished and electronic conductivity increased with chromium content.

In recent years, there has been much interest in the development of ionic conductors for potential use as solid electrolytes or cathodes in lithium batteries. For a long time research has been focused on doping compounds such as Li_4XO_4 and Li_3YO_4 (X = Si, Ge, Ti; Y = P, As, V).[1–5] A few years ago, fast ion conductors with the general formula $Li_{0.5-3x}RE_{0.5+x}TiO_3$ (RE = La, Pr, Nd, Sm) were reported.[6–12] The maximum bulk ionic conductivity is found in the lanthanum system, with a value of 1.1×10^{-3} S cm^{-1} for $x=0.07$, although the total ionic conductivity was less than 10^{-6} S cm^{-1}. Recently, the phase diagram, crystal chemistry and ion conductivity of $Li_{0.5-3x}Pr_{0.5+x}TiO_3$ systems have been reported.[10] The aim of the present work was to investigate the stoichiometry range, thermal stability, crystal chemistry and electrical behavior of materials of general formula $Pr_{0.5+x+y}Li_{0.5-3x}Ti_{1-3y}Cr_{3y}O_3$.

Experimental

Pr_6O_{11} (99.9%, Fluka), TiO_2 (Aldrich, 99+%), Cr_2O_3 (>99%, Fluka) and Li_2CO_3 (>99%, Aldrich) were used as starting materials. Pr_6O_{11} and TiO_2 were dried overnight at 900 °C prior to weighing. These chemicals were weighed, mixed in an agate mortar with acetone, dried and heated at 650 °C for 2 h to drive off CO_2. After grinding, samples were pressed into pellets and covered with a powder of the same composition to avoid losing lithium during thermal treatment. The pellets were fired at 1100 °C for 8 h giving green products which were reground, repelleted and fired at 1150 and 1200 °C for 12 h. A further treatment was carried out on samples richer in praseodymium at 1250 °C to widen the single phase region.

Phase diagram studies *vs.* temperature were carried out for some compounds. Small pelleted samples were wrapped in platinum foil envelopes, placed in a furnace and annealed isothermally for 15 min in order to reach equilibrium. Finally they were immersed in liquid nitrogen to quench the phase distribution.

The solid solution range, crystalline phase identification and lattice parameters were obtained by powder X-ray diffraction with a Siemens D-500 diffractometer in reflection mode and an INEL ENRAF NONIUS FR590 diffractometer in transmission mode with a psd-120° detector and graphite monochromator, using Cu-Kα radiation. Lattice parameters were obtained using a silicon internal standard.

Some samples were studied by electron probe microanalysis (EPMA) to check homogeneity with a Cameca SX50 EPMA instrument. Element maps were obtained with an AN10000 EDS instrument coupled to a JEOL JSM-840 microscope. Stoichiometries were obtained by ICP-AAS with a JOVIN IVON instrument. DC measurements were carried out using a HP 3435A multimeter, and AC measurements with a HP 4192A Impedance Analyser over the range $5\ \text{Hz} < f < 1.3\times10^7$ Hz. Data corrections were carried out in order to avoid stray inductance, although data above 5×10^6 Hz were discarded.

Results and Discussion

The triangle $PrCrO_3$–$Pr_{0.5}Li_{0.5}TiO_3$–$Pr_{2/3}TiO_3$ in the system Li_2O–Pr_6O_{11}–TiO_2–Cr_2O_3 was chosen for detailed study since the $Pr_{0.5}Li_{0.5}TiO_3$–$Pr_{2/3}TiO_3$ join has been previously reported[9] and $PrCrO_3$ has a similar structure[13] to compounds on this join. This triangle was studied by synthesizing compositions of general formula $Li_{0.5-3x}Pr_{0.5+x+y}Ti_{1-3y}Cr_{3y}O_3$ under heating conditions as described above. The results were used to construct the composition diagram (Fig. 1).

Three distinct areas were found on this triangle: a region of

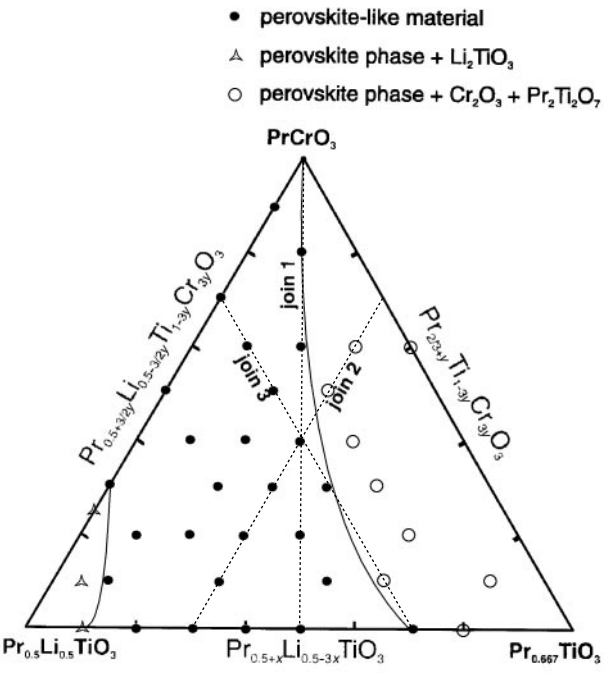

Fig. 1 Composition triangle and joins studied of the system $Pr_{0.5+x+y}Li_{0.5-3x}Ti_{1-3y}Cr_{3y}O_3$

†E-mail: mluisa@kripto.qui.ub.es

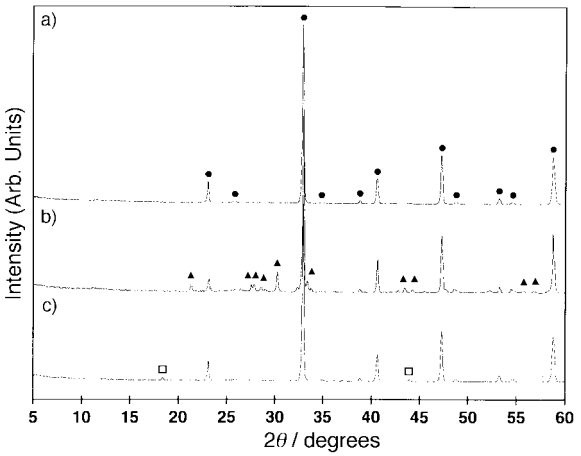

Fig. 2 XRD patterns of the three regions on the composition triangle: (a) single phase solid solution region, (b) perovskite-like phase (●) + $Pr_2Ti_2O_7$ (▲) region, and (c) perovskite-like phase (●) + Li_2TiO_3 (□) region

perovskite-like solid solutions and two mixed phase regions. Almost all the right half of the triangle was a mixture of the perovskite-like phase and $Pr_2Ti_2O_7$–Cr_2O_3–TiO_2 [Fig. 2(b)]. However, a perovskite-like solid solutions area [Fig. 2(a)] was also found in the left side, except for a small area within the vertex $Pr_{0.5}Li_{0.5}TiO_3$, which was a mixture of the perovskite phase and Li_2TiO_3 [Fig. 2(c)].

EPMA and elemental maps

A selection of ceramic samples, from both within and outside the perovskite single phase region, was analysed by EPMA and SEM/EDS. The analyses took the form of either elemental maps for Pr, Cr and Ti, or point analyses for Pr, Cr, Ti and O. Elemental maps were obtained for samples from each of the three regions observed in the composition triangle. Fig. 3

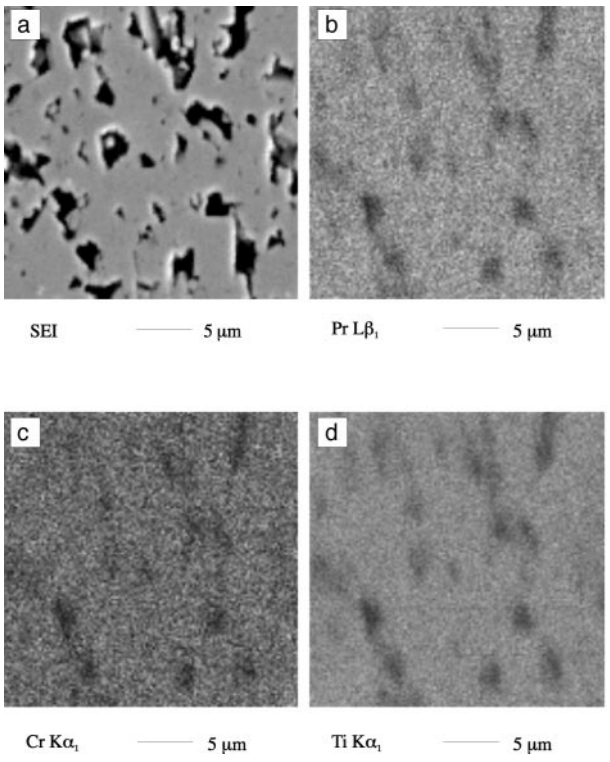

Fig. 3 SEM image and elemental maps for $Pr_{0.75}Li_{0.35}Ti_{0.60}Cr_{0.40}O_3$ (single phase region): (a) SEM, (b) elemental map of Pr, (c) map of Cr and (d) map of Ti

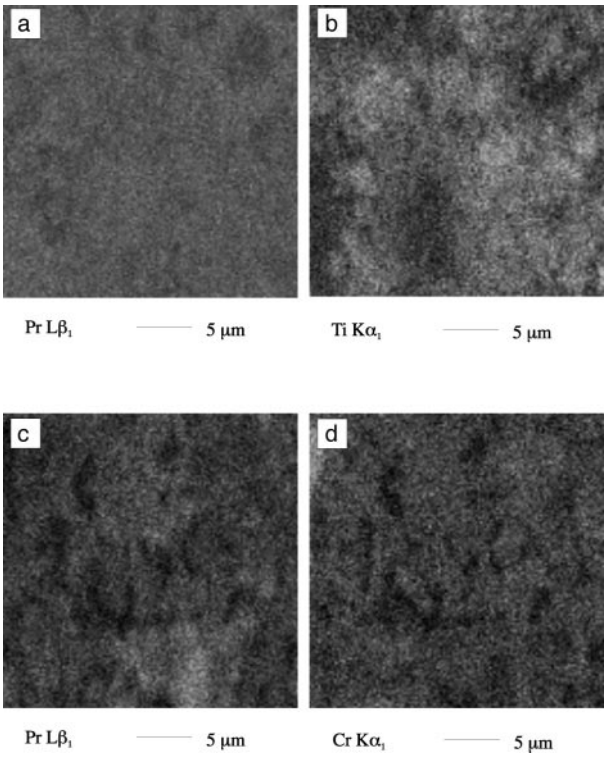

Fig. 4 Elemental maps of multiphase regions: (a) map of Pr and (b) map of Ti of $Pr_{0.558}Li_{0.425}Ti_{0.90}Cr_{0.10}O_3$ sample, and (c) map of Pr and (d) map of Cr of $Pr_{0.667}Li_{0.10}Ti_{0.60}Cr_{0.40}O_3$ sample

shows an SEM image and Pr, Cr and Ti maps for $Pr_{0.75}Li_{0.35}Ti_{0.60}Cr_{0.40}O_3$. Only one phase, with a homogeneous element distribution, was found.

A similar study was carried out on the multiphase regions. Fig. 4(a) and (b) show elemental maps for a Li-rich sample, $Pr_{0.558}Li_{0.425}Ti_{0.90}Cr_{0.10}O_3$, which is clearly composed of two phases. In Fig. 4(a), a grayish area corresponds to a perovskite compound and lighter areas in the Ti elemental map [Fig. 4(b)] were attributed to Li_2TiO_3. Elemental maps for $Pr_{0.667}Li_{0.10}Ti_{0.60}Cr_{0.40}O_3$ [Fig. 4(c) and (d)] showed three regions. The largest region corresponds to a perovskite compound, while lighter spots in the Cr map [Fig. 4(d)] were attributed to Cr_2O_3 and light regions in the Pr map [Fig. 4(c)] to $Pr_2Ti_2O_7$.

Element analyses were carried out with a fixed beam of 15 kV and 20 nA. The Pr, Cr, Ti and O contents were determined for 12 points in each sample using $SrTiO_3$, PrF_3 and Cr_2O_3 as standards. Results are shown in Table 1 with the Cr + Ti amount set as unity and the remaining values renormalised in the formula $Pr_{0.5+x+y}Li_{0.5-3x}Ti_{1-3y}Cr_{3y}O_3$. For all compositions, the Pr : Ti : Cr ratios were in good agreement with the expected values for the starting compositions. Lithium content could not be obtained directly and so had to be calculated by assuming three oxygen atoms per unit formula and valencies of 3+ for Pr and Cr, and 4+ for Ti. Experimental values of oxygen contents have larger uncertainties than the values for Pr, Ti and Cr due to the difficulty in separating the O Kα signal from that emitted by the carbon coating and partial absorption of the O Kα signal by the carbon. $SrTiO_3$, which was the standard for oxygen, and samples of the single phase region were coated together to improve the oxygen measurements.

Phase diagram and crystal chemistry

Phase diagrams and cell volume were obtained for three joins on the composition triangle (Fig. 1). Along join 1 [$Pr_{0.538}Li_{0.25}TiO_3$–$PrCrO_3$] lithium, praseodymium, chro-

Table 1 Element analyses (EPMA) of $Pr_{0.5+x+y}Li_{0.5-3x}Ti_{1-3y}Cr_{3y}O_3$ in the single phase region

$Pr_{0.5+x+y}Li_{0.5-3x}Ti_{1-3y}Cr_{3y}O_3$		starting compositions				experimental compositions			
x	y	Pr	Ti	Cr	Li	Pr	Ti	Cr	O
0.080	0.000	0.580	1.000	0.000	0.250	0.582(9)	1.00(1)	0.000	2.99(5)
0.117	0.133	0.750	0.600	0.400	0.150	0.743(5)	0.609(6)	0.39(1)	3.07(6)
0.167	0.333	1.000	0.000	1.000	0.000	1.009(7)	0.000	1.00(2)	3.03(4)
0.083	0.133	0.623	0.600	0.400	0.250	0.623(8)	0.610(8)	0.391(7)	3.06(6)
0.100	0.067	0.800	0.800	0.200	0.200	0.790(6)	0.792(8)	0.208(9)	2.94(5)

mium and titanium compositions and the number of vacancies changed, while along join 2 [$Pr_{0.55}Li_{0.35}TiO_3$–$Pr_{0.90}Ti_{0.30}Cr_{0.70}O_3$] the number of vacancies was constant, and along join 3 [$Pr_{0.617}Li_{0.15}TiO_3$–$Pr_{0.85}Li_{0.15}Ti_{0.30}Cr_{0.70}O_3$] the amount of lithium was constant.

Three polymorphs, labelled A, C and β, by analogy with similar polymorphs in the $RE_{0.5+x}Li_{0.5-3x}TiO_3$ (RE = Pr, Nd)[9,10] systems, were identified. These three polymorphs have perovskite-related structures. Polymorph A is a simple cubic perovskite (Table 2) and polymorph C (Table 3) is an orthorhombic distortion of A, with a unit cell which is approximately four times larger. The cells of A and C are related by: $a_o = \sqrt{2}a_c + \delta$, $b_o = 2a_c$, and $c_o = \sqrt{2}a_c - \delta$, where a_c is the cell parameter of the cubic A phase and δ is the degree of orthorhombicity. Polymorph β is a tetragonal perovskite with unit cell: $a_o = a_c - \delta$ and $c_o = 2a_c + \Delta$ (Table 4).

Along joins 1 and 3, polymorphs A and C only form at high temperatures. Although these phases are stable at high temperatures, they can be preserved at room temperature by quenching. Phase C extends over a shorter composition range than in $Pr_{0.5+x}Li_{0.5-3x}TiO_3$ and $La_{0.5+x+y}Li_{0.5-3x}Ti_{1-3y}Mn_{3y}O_3$ systems.[10,14] Polymorph β extends along the whole range of compositions at low temperatures (Fig. 5). Along join 3, only polymorphs A and β are present since for a short number of vacancies the perovskite phase decomposed to give phase A or β, Cr_2O_3 and $Pr_2Ti_2O_3$.

The cell volume was measured against the amount of praseodymium along these three joins (Fig. 6) and was found to increase whenever the praseodymium content increased, while for the same amount of praseodymium, it decreased as the lithium content increased. Since both lithium and praseodymium should be in 12-coordinated sites, steric effects are predominant in praseodymium substitution, making cells larger, while electrostatic interactions between lithium and octahedra MO_6 (M = Ti or Cr) are more important in lithium substitution, with the reverse effect on the cells.

Table 2 X-Ray powder diffraction data for $Pr_{0.667}Li_{0.20}Ti_{0.80}Cr_{0.20}O_3$ quenched from 1100 °C (phase A)

$h\ k\ l$	d_{obs}/Å	d_{calc}/Å	I/I_o
1 0 0	3.8411	3.8463	7
1 1 0	2.7172	2.7198	100
1 1 1	2.2193	2.2207	18
2 0 0	1.9224	1.9232	32
2 1 0	1.7196	1.7201	4
2 1 1	1.5701	1.5703	35
2 2 0	1.3601	1.3599	21
3 0 0	1.2824	1.2821	2
3 1 0	1.2167	1.2163	15

Cubic system: $a_o = 3.8463(9)$ Å, $V = 56.902(3)$ Å^3, $Z = 1$.

Table 3 X-Ray powder diffraction data for $Pr_{0.917}Li_{0.05}Ti_{0.20}Cr_{0.80}O_3$ quenched from 1100 °C (phase C)

$h\ k\ l$	d_{obs}/Å	d_{calc}/Å	I/I_o
0 2 0	3.8589	3.8554	24
2 0 0	2.7299	2.7285	100
1 2 1	2.7222	2.7259	35
2 1 1	2.3259	2.3258	3
1 1 2	2.3231	2.3232	1
2 2 0	2.2273	2.2271	21
0 2 2	2.2231	2.2241	5
1 3 1	2.1388	2.1385	2
0 4 0	1.9281	1.9277	38
2 3 0	1.8717	1.8709	6
3 1 0	1.7686	1.7704	1
3 0 1	1.7249	1.7253	8
2 2 2	1.7233	1.7239	2
3 1 1	1.6834	1.6836	2
3 2 1	1.5744	1.5748	57
3 3 1	1.4324	1.4325	1
4 0 0	1.3639	1.3642	18
4 1 0	1.3447	1.3434	5
4 1 1	1.3044	1.3043	<1
1 1 4	1.3022	1.3020	<1
4 2 0	1.2859	1.2861	3
0 6 0	1.2850	1.2851	1
0 2 4	1.2839	1.2838	<1
4 0 2	1.2198	1.2197	15

Orthorhombic system: $a_o = 5.4569(8)$ Å, $b_o = 7.711(2)$ Å, $c_o = 5.446(1)$ Å, $V = 229.140(4)$ Å^3, $Z = 4$.

Electrical measurements (AC/DC)

AC and DC measurements were carried out from 25–200 °C for compounds on join 1 using gold electrodes. Samples were pressed into pellets (diameter ≈6 mm and thickness ≈2 mm), and sintered at 1250 °C for 1 h. Pellet sides were sanded and painted with gold paste (Engelhard T-10112) which was fixed in a tubular furnace with a maximum temperature of 900 °C.

Along join 1, three types of behavior were observed (Fig. 7).

Table 4 X-Ray powder diffraction data for $Pr_{0.75}Li_{0.15}Ti_{0.60}Cr_{0.40}O_3$ quenched from 800 °C (phase β)

$h\ k\ l$	d_{obs}/Å	d_{calc}/Å	I/I_o
0 0 2	3.8780	3.8523	13
1 0 0	3.8457	3.8485	15
0 1 1	3.4450	3.4429	4
1 0 2	2.7242	2.7226	100
1 1 0	2.7208	2.7213	18
0 0 3	2.5697	2.5682	2
1 1 2	2.2228	2.2227	20
0 1 3	2.1346	2.1362	1
0 0 4	1.9251	1.9261	21
1 1 3	1.8687	1.8678	3
1 0 4	1.7224	1.7225	5
2 0 2	1.7186	1.7214	1
1 2 1	1.6780	1.6797	2
1 1 4	1.5724	1.5722	37
1 2 2	1.5695	1.5714	10
0 1 5	1.4314	1.4305	1
1 2 3	1.4288	1.4297	1
0 2 4	1.3603	1.3613	10
0 0 6	1.2838	1.2841	4
1 0 6	1.2180	1.2181	18
2 2 3	1.2041	1.2023	1
1 3 1	1.2028	1.2021	<1

Tetragonal system: $a_o = 3.849(1)$ Å, $c_o = 7.705(2)$ Å, $V = 114.112(3)$ Å^3, $Z = 2$.

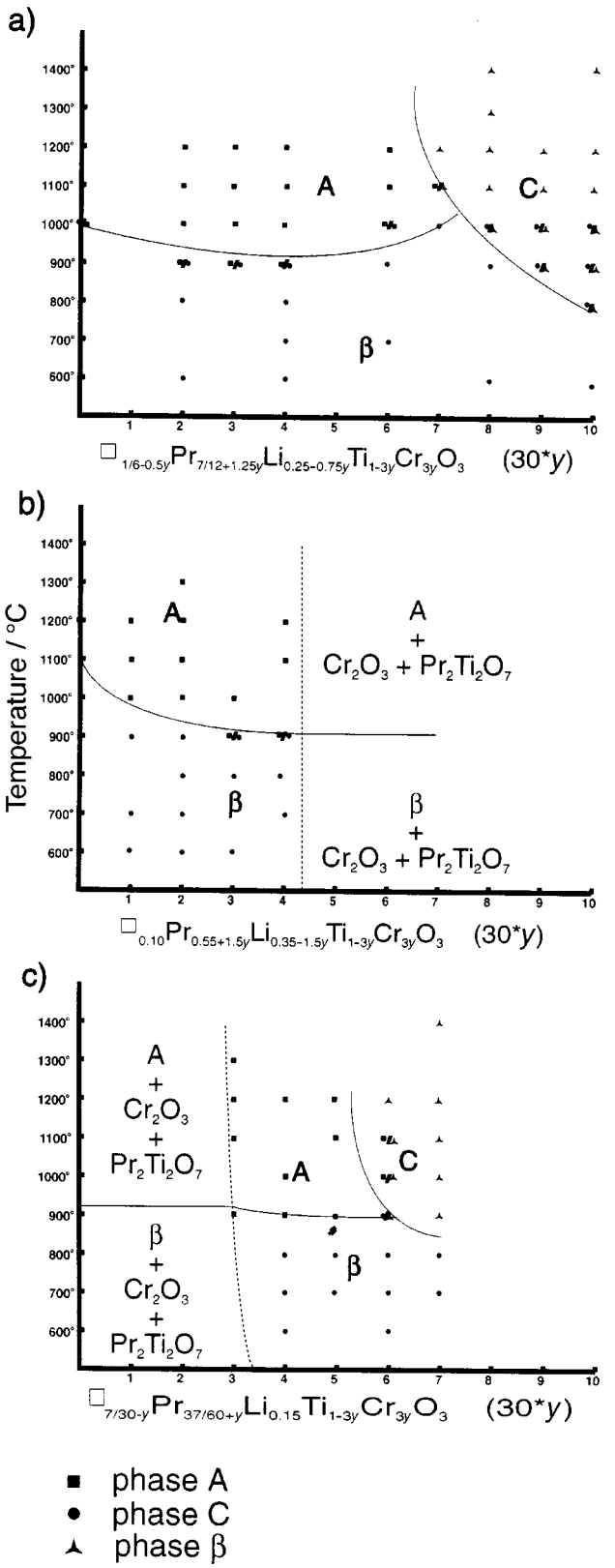

Fig. 5 Phase diagrams along each join: (a) $Pr_{0.538}Li_{0.25}TiO_3$–$PrCrO_3$ (b) $Pr_{0.55}Li_{0.35}TiO_3$–$Pr_{0.90}Ti_{0.30}Cr_{0.70}O_3$, and (c) $Pr_{0.617}Li_{0.30}TiO_3$–$Pr_{0.85}Li_{0.15}Ti_{0.30}Cr_{0.70}O_3$

For $y=0.0$ [Fig. 7(a)], two semicircles and a spike were observed which are related to ionic conductivity. The centre of these semicircles was depressed below the baseline, indicating a non-Debye response, which is usual in ionic conductors.[14–16] The first and second semicircle showed capacities around 3 pF and 2 nF therefore they are related to bulk and grain boundaries,[1] while the spike had a capacity around 50 nF. This

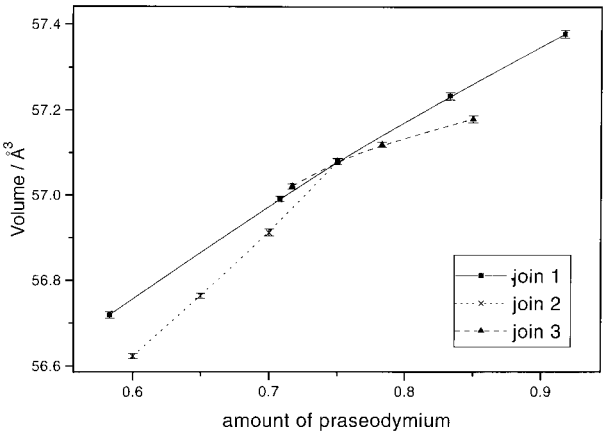

Fig. 6 Cell volume *vs.* praseodymium content along the three joins on samples quenched from 1000 °C

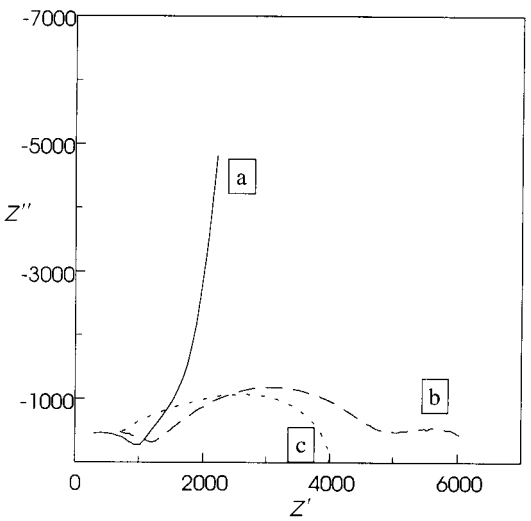

Fig. 7 Impedance response at 200 °C for: (a) $Pr_{0.583}Li_{0.25}TiO_3$, (b) $Pr_{0.666}Li_{0.20}Ti_{0.80}Cr_{0.20}O_3$, (c) $Pr_{0.75}Li_{0.15}Ti_{0.6}Cr_{0.4}O_3$

value, which is too low for an electrode, has been previously reported for high Na^+ and Li^+ ion conductors[10,16] and it is attributed to the presence of a Na^+- or Li^+-free layer on the crystal surface. For $0<y\leqslant0.10$ [Fig. 7(b)], compounds were mixed conductors with greater ionic than electronic conductivity and three semicircles were observed with capacities close to 2 pF, 2 nF and 5 μF. The third semicircle became smaller as the electronic conductivity was increased. Finally, for $y>0.10$ [Fig. 7(c)], electronic conductivity was greater than ionic conductivity, and only two overlapped semicircles were observed with capacities around 5 pF and 1 nF.

An equivalent circuit (Fig. 8) with two parallel branches, one of them related to ionic conductivity and the other one to electronic conductivity, was used to fit the experimental measurements. The electronic part comprised two *RC* elements associated with grain and grain boundary responses, while the ionic part was made of two *RC* elements with two CPE[17] (constant phase elements) for grain and grain boundary response and an additional CPE element to model a blocking electrode for lithium ions. All fitting used the Zview software package.[18]

Bulk ionic conductivity data from the impedance complex plane plots are shown in Arrhenius format. Plots are linear and the conductivity decreased as the amount of lithium diminished (Fig. 9). The variation in ionic conductivity with lithium composition is quite small (Fig. 10), while the activation energy was from 0.470–0.453 eV.

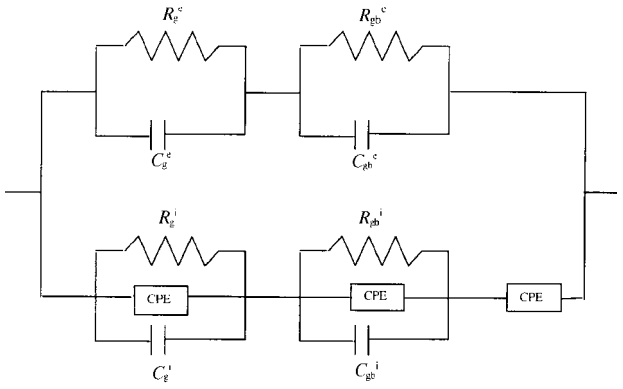

Fig. 8 Equivalent circuit for fitting AC data and fitting result for $Pr_{0.666}Li_{0.20}Ti_{0.8}Cr_{0.2}O_3$ (175 °C) [$R_b^e = 7.9(9) \times 10^3\ \Omega$ cm, $C_b^e = 1.7(1) \times 10^{-12}$ F cm^{-1}, $R_b^i = 3.32(1) \times 10^3\ \Omega$ cm, $C_b^i = 2.7(1) \times 10^{-12}$ F cm^{-1}, $T = 1.9(1) \times 10^{-8}$ S cm^{-1}, $n = 0.57(3)$; $R_{gb}^e = 4.5(5) \times 10^3\ \Omega$ cm, $C_{gb}^e = 2.2(1) \times 10^{-9}$ F cm^{-1}, $R_{gb}^i = 3.25(6) \times 10^4\ \Omega$ cm, $C_{gb}^i = 8.3(2) \times 10^{-10}$ F cm^{-1}, $T = 3.1(3) \times 10^{-7}$ S cm^{-1}, $n = 0.52(2)$; $T = 1.4(1) \times 10^{-6}$ S cm^{-1}, $n = 0.73(3)$. CPE equation: $Y = T\cos(n\pi/2)\omega^n + T\sin(n\pi/2)\omega^n$]

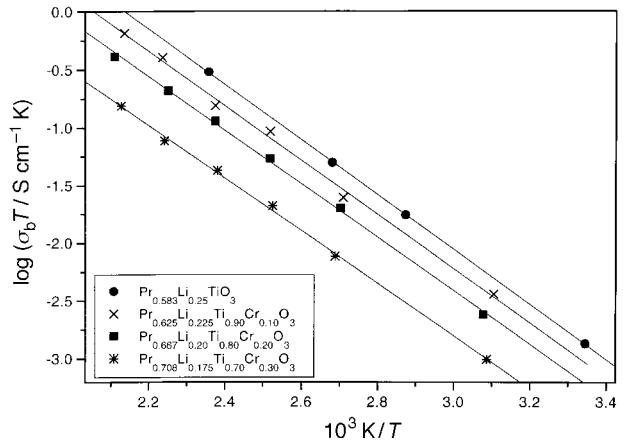

Fig. 9 Arrhenius ionic conductivity plots

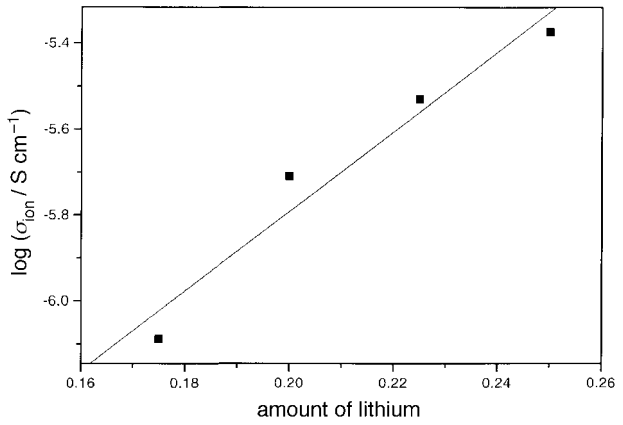

Fig. 10 Plot of log σ (bulk ionic conductivity) at 25 °C *vs.* lithium content composition

Overall electronic conductivity, DC measurements, showed that samples doped with chromium became mixed conductors; electronic conductivity is dependent on chromium content (Fig. 11). Electronic conductivity increased with increasing amounts of chromium. Both the ionic and the electronic conductivity were close to $10^{-6}\ \Omega^{-1}$ cm^{-1} for $y = 0.10$.

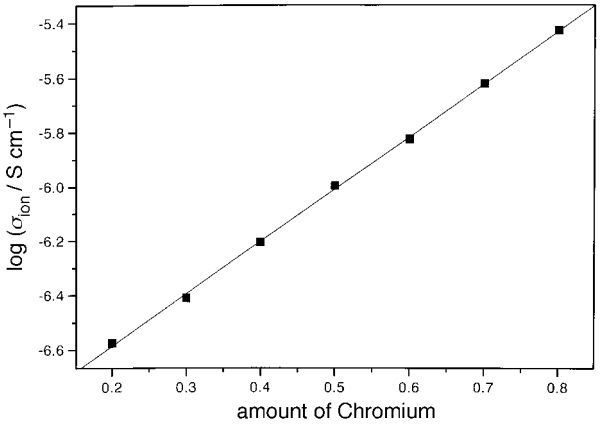

Fig. 11 Plot of σ (overall electronic conductivity) at 25 °C *vs.* chromium content

Conclusions

A large range of single phase solid solutions have been synthesized in the triangle $PrCrO_3$–$Pr_{0.5}Li_{0.5}TiO_3$–$Pr_{2/3}TiO_3$. The phase diagram in the single phase region showed the existence of three polymorphs with perovskite-like structures, labelled as A, C, and β. Polymorph A has a cubic perovskite structure, C is an orthorhombic distortion of A with a cell four times that of A, and β a tetragonal phase with a double cell.

Cell volume increased whenever the praseodymium content increased. Nevertheless, it decreased as the lithium content increased for the same amount of praseodymium. This is attributable to an electrostatic interaction between the lithium ions and negatively charged octahedra that shrunk the cell.

AC/DC measurements indicated that these compounds are mixed conductors. Li^+ ion conductivity decreased as the amount of lithium diminished, meanwhile electronic conductivity increased with the amount of chromium.

This work was sponsored by financial support from CICYT MAT-95-0218.

References

1 J. T. S. Irvine and A. R. West, in *High Conductivity Solid Ionic Conductors*, Recent Trends and Applications, ed. T. Takalashi, World Scientific, Singapore, 1989, pp. 201–222.
2 H. Y. P. Hong, *Mater. Res. Bull.*, 1978, **13**, 117.
3 M. A. K. L. Dissanayake and A. R. West, *J. Mater. Chem.*, 1991, **1**, 1023.
4 C. K. Lee and A. R. West, *J. Mater. Chem.,* 1991, **1,** 149.
5 A. Robertson and A. R. West, *Solid State Ionics*, 1992, **58**, 351.
6 M. Itoh, Y. Inaguma, W. Jung, L. Chen and T. Nakamura, *Solid State Ionics*, 1994, **70/71**, 203.
7 H. Kawai and J. Kuwano, *J. Electrochem. Soc.*, 1994, **141**, L78.
8 Y. Inaguma, L. Chen, M. Itoh and T. Nakamura, *Solid State Ionics*, 1994, **70/71**, 196.
9 A. D. Robertson, S. García Martín, A. Coats and A. R. West, *J. Mater. Chem.*, 1995, **5**, 1405.
10 M. Morales and A. R. West, *Solid State Ionics*, 1996, **84**, 33.
11 J. M. S. Skakle, G. C. Mather, M. Morales, R. I. Smith and A. R. West, *J. Mater. Chem.*, 1995, **5**, 1807.
12 R. I. Smith, J. M. S. Skakle, G. C. Mather, M. Morales and A. R. West, *Mater. Sci. Forum*, 1996, **228–231**, 701.
13 A. Roy and J. Nag, *J. Inorg. Chem.*, 1978, **40**, 1501.
14 I. Moreno, M. Morales and M. L. Martínez Sarrión, *J. Solid State Chem.*, in press.
15 A. K. Jonscher and J. M. Reau, *J. Mater. Sci.*, 1978, **13**, 563.
16 P. G. Bruce, A. R. West and D. P. Almond, *Solid State Ionics*, 1982, **7**, 57.
17 A. K. Jonscher, in *Dielectric Relaxation in Solids*, Chelsea Dielectric Press, London, 1983, ch. 5.
18 Zview for Windows (ver. 1.4), Scribner Assoc. Inc., Charlotesville, Virginia, USA.

Paper 8/00752G; *Received* 28*th January*, 1998